Supplementary Materials for Universal $2\Delta_{max}/k_BT_c$ scaling decoupled from the Electronic Coherence in Iron-Based Superconductors

H. Miao,[1,2,*] W. H. Brito,[2] Z. P. Yin,[3] R. D. Zhong,[2] G. D. Gu,[2] P. D. Johnson,[2] M. P. M. Dean,[2] S. Choi,[2] G. Kotliar,[2,4] X. C. Wang,[1] C. Q. Jin,[1] S. -F. Wu,[1] T. Qian,[1] and H. Ding[1,5,†]

[1] *Beijing National Laboratory for Condensed Matter Physics, Institute of Physics, Chinese Academy of Sciences, Beijing 100190, China*
[2] *Condensed Matter Physics and Materials Science Department, Brookhaven National Laboratory, Upton, New York 11973, USA*
[3] *Department of Physics and the Center of Advanced Quantum Studies, Beijing Normal University, Beijing 100875, China*
[4] *Department of Physics and Astronomy, Rutgers University, Piscataway, New Jersey 08854, USA*
[5] *Collaborative Innovation Center of Quantum Matter, Beijing 100190, China*

(Dated: June 22, 2018)

SAMPLE PREPARATION.

High-quality $FeTe_{0.55}Se_{0.45}$ single crystals were grown by a unidirectional solidification method with a nominal composition of $FeTe_{0.55}Se_{0.45}$ (T_c = 14.5 K and ΔT_c=1 K). Single crystals of LiFeAs (T_c = 18 K and ΔT_c=1 K) were synthesized by a self-flux method using Li_3As, FeAs, and As powders as the starting materials. The mixture was ground and put into an alumina crucible and sealed in an Nb crucible under 1 atm of argon gas. The Nb crucible was then sealed in an evacuated quartz tube, heated to 1100°C, and slowly cooled down to 700°C at a rate of 3°/h.

BAND DISPERSION

The normal state band dispersion that is determined by ARPES. In order to increase the number of photoelectron and prevent surface aging, the measurement was performed with medium energy resolution ($\sim$ 10 meV) at 30 K. Figures 1a and b show the second derivative of ARPES intensity map along Γ (0,0)-M (π,0) direction of LiFeAs and $FeTe_{0.55}Se_{0.45}$, respectively. Here we use the 1 Fe per unit cell notation. The colorscale of these two plots are the same. The intensity contrast in LiFeAs is much larger than $FeTe_{0.55}Se_{0.45}$, consistent with the Fermi liquid normal state of LiFeAs and bad metal normal phase of $FeTe_{0.55}Se_{0.45}$. We note that compare with the LDA+DMFT calculation shown in Fig. 2b of the main text, the shallow electron pocket at the Γ point in $FeTe_{0.55}Se_{0.45}$ is not evident in our raw data, but has been clearly observed in laser-ARPES with improved momentum resolution [1, 2].

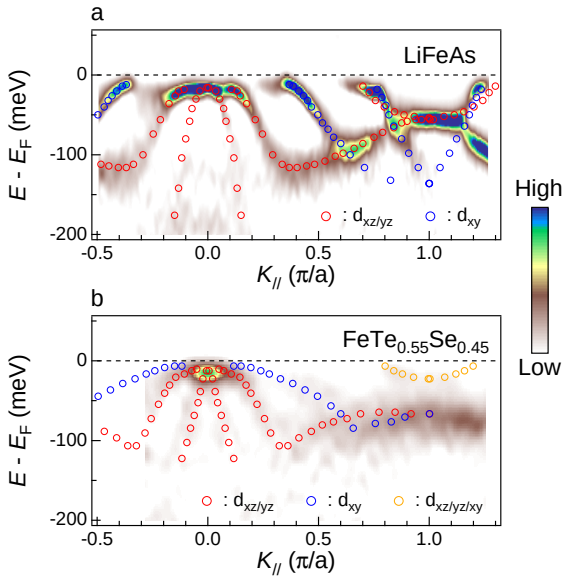

Figure 1. Second derivative of ARPES intensity map along Γ-M direction of (a) LiFeAs and (b) $FeTe_{0.55}Se_{0.45}$. Colored circles are the extracted band dispersion. Near E_F, the dispersion is extracted by tracing the EDC peak positions. At higher energy, band dispersion is directly extracted from the second derivative plot and consistent with previous studies [1, 3, 4]. The data point at $k_{//} < 0$ is symmetrized from the data point at $k_{//} > 0$. The orbital contributions of each band are represented by different colors.

FERMI ENERGY IN THE IRON-BASED SUPERCONDUCTORS

In single band and single orbital electronic systems, the quasi-particle (QP) kinetic energy can be written as $E_K = \frac{\hbar^2 k^2}{2m^*}$ and m^* is the effective mass, therefore the Fermi energy, E_F, is corresponding to the band top or band bottom of the valence band. In the multi-band and multi-orbital FeSCs, the same electron, say the d_{xy} electron, is contributing for both the electron bands at

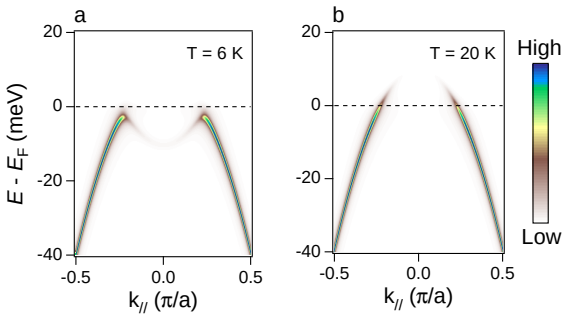

Figure 2. Simulated BCS spectral function $A(k,\omega)$ at (a) 6 K and (b) 20 K. The colorscale of (a) and (b) are the same.

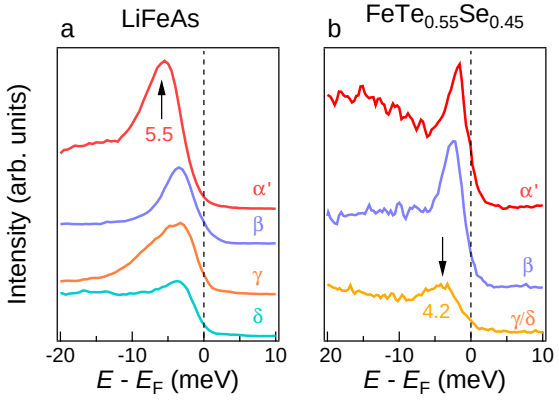

Figure 3. ARPES measured SC gap on (a) LiFeAs and (b)$FeTe_{0.55}Se_{0.45}$. The largest SC gap (5.5±0.3 meV) in LiFeAs is observed on the α' band near the Γ point, while the largest SC gap (4.2±0.3 meV) in $FeTe_{0.55}Se_{0.45}$ is observed on the electron band.

the M point and the hole bands at the Γ point with the total QP kinetic energy $E_K^{xy} = \sum \frac{\hbar^2 k_i^2}{2m_i^{xy*}}$. Therefore it is natural using E^{tot} to describe E_F. Here E^{tot} is defined as the largest energy difference between the bottom of the electron bands at the M point and the top of the hole bands at the Γ point. Since ARPES can only measure occupied states, the band top of hole bands at the Γ point is determined by using a parabolic function, $a + bk^2$, to fit the band dispersion in the occupied state. In LiFeAs, we found $a^{xy} = 50\pm5$ meV, combined with the experimentally determined band bottom at the M point yields $E^{tot}_{LiFeAs} \sim 200$ meV. In $FeTe_{0.55}Se_{0.45}$, we found $a^{xy} = 3 \pm 2$ meV, combined with the experimentally determined band bottom at the M point yields $E^{tot}_{FTS} \sim 25$ meV.

We shall note that, E_F is also expected to be orbital dependent. However, as we shown in Fig. 1, in FeSCs, E_{tot} is similar for all t_{2g} bands. Therefore, the E_{tot} can be considered as an averaged E_F for the t_{2g} bands. As we described in the main text, this definition can precisely reproduce the recently observed Caroli-de Gennes-Martricon states in $FeTe_{0.55}Se_{0.45}$ [5] and more consistent with previous ARPES data in $LiFe_{1-x}Co_xAs$ [6].

THE BCS SPECTRAL FUNCTION

Figures 2a and b show the simulated BCS spectral function at 6 K and 20 K, respectively.

$$A(k,\omega) = \frac{1}{2}\Big[\frac{\Gamma_k(1+\frac{\xi_k}{E_k})}{(\omega - E_k)^2 + \Gamma_k^2} + \frac{\Gamma_k(1-\frac{\xi_k}{E_k})}{(\omega + E_k)^2 + \Gamma_k^2}\Big] \quad (1)$$

with

$$E_k = \sqrt{\xi_k^2 + \Delta_k^2} \quad (2)$$

Here we use a parabolic band dispersion, $\xi_k = 10 - 200 \times k^2$ and set $\Gamma_k = 1$ meV and $\Delta_k = 3$ meV. Since Eq. 1 mixes particle and hole in the superconducting (SC) phase, the Bogliubov dispersion that is described by Eq. 2 can only be observed at $k < k_F$ for hole-like band. This is fully consistent with LiFeAs, where the Bogliubov QP peak is indeed observed at $k < k_F$ and is absent at $k > k_F$ (Fig. 2c of the main text). In $FeTe_{0.55}Se_{0.45}$, however, a coherent QP peak that is associate with superconductivity is observed at $k > k_F$. This non-BCS behavior is a strong spectroscopic evidence to prove that the coherent SC spectral weight emerges directly from an intrinsically incoherent bad metal phase [7, 8].

THE SUPERCONDUCTING GAP ON DIFFERENT ELECTRONIC BAND

In iron-based superconductors (FeSCs), SC gaps on different electronic bands are different. Figure 3 shows the ARPES determined SC gap in LiFeAs and $FeTe_{0.55}Se_{0.45}$. All EDCs are measured at 6 K. In LiFeAs, k_F positions of the electronic bands are determined by momentum distribution curve (MDC) in the normal state at E_F. In $FeTe_{0.55}Se_{0.45}$, due to the bad metal normal state, k_F positions are determined by the gap-minimum positions in the superconducting state. In LiFeAs, the largest SC gap is observed on the α' band, which is mainly composed of d_{xz}/d_{yz} orbital characters. In contrast, the largest SC gap in $FeTe_{0.55}Se_{0.45}$ is observed on the electron band, where all three t_{2g} orbitals have large contribution.

UNIVERSAL Δ_{max}/T_c SCALING

ARPES determined Δ_{max}			
Materials	Δ_{max} (meV)	T_c (K)	$2\Delta_{max}/T_c$
$BaFe_{1.85}Co_{0.15}As_2$[9]	7±1	25.5	6.4±0.9
$Ba_{0.75}K_{0.25}Fe_2As_2$[10]	8±0.8	26	7.12±0.72
$Ba_{0.6}K_{0.4}Fe_2As_2$[11]	12±1.5	38	7.32±0.9
$Ba_{0.3}K_{0.7}Fe_2As_2$[10]	7.9±0.8	22	8.32±0.72
$Ba_{0.1}K_{0.9}Fe_2As_2$[12]	3.6±0.5	10	8.34±1.2
$BaFe_{1.5}Ru_{0.5}As_2$[13]	5.5±0.8	15	8.5±1.2
$BaFe_2As_{1.4}P_{0.6}$[14]	8.6±0.8	30	6.7±0.62
LiFeAs[6]	5.5±0.5	18	7.08±0.64
$LiFe_{0.97}Co_{0.03}As$[6]	4.5±0.5	15	6.96±0.76
$FeTe_{0.55}Se_{0.45}$[15]	4.2±0.5	14.5	6.72±0.8
$NaFe_{0.95}Co_{0.05}As$[16]	6.5±1	18	8.36±1.2
KFe_2Se_2[17]	8.5 ±1	29	6.8±0.8
FeSe[18]	3.0 ±0.5	8	8.6±1.5

DFT+DMFT CALCULATIONS FOR THE $FeTe_{0.55}Se_{0.45}$ ALLOY

In $FeTe_{0.55}Se_{0.45}$, although Te:Se∼1:1, it does not form any charge or magnetic order. This is consistent with STM and ARPES studies [15, 19], where no superstructure or band-folding is observed. Therefore to investigate the $FeTe_{0.55}Se_{0.45}$ alloy we construct a model starting from the crystal structure of pristine FeSe. As shown in Fig. 4, in our model we considered that the main effect of alloying Te and Se is the increasing of the chalcogen height. To take this effect into account we considered that the Se height in our model is the average height of Se and Te in pristine FeSe (1.475 Å) and FeTe (1.755 Å), respectively. As a result, in our model the Se height is taken to be $\Delta = 1.615$ Å. It is noteworthy that within our model we neglect the additional effects of alloying Te and Se, such as structural disorder, those effects are expected to further decrease the coherence of the electronic state.

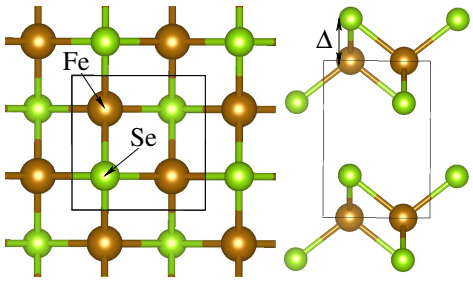

Figure 4. Top and side views of our structural model for the $FeTe_{0.55}Se_{0.45}$ alloy. In our model the Se height is $\Delta = 1.615$ Å. The brown and green spheres represent Fe and Se atoms, respectively. The unit cell is represented by the rectangular prism.

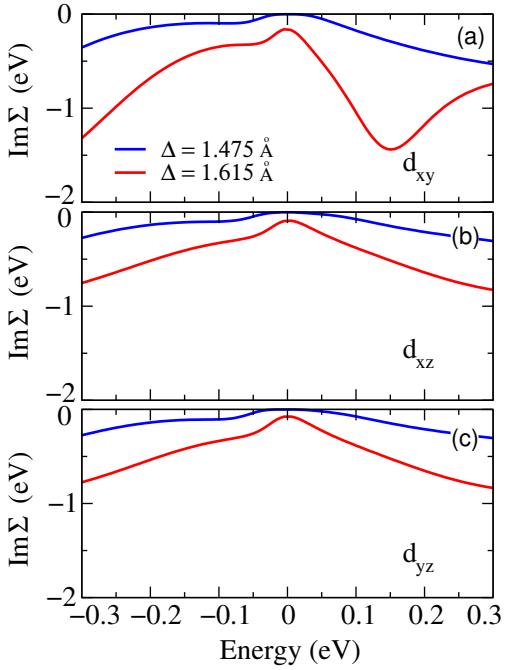

Figure 5. Imaginary part of DMFT self-energy of (a) d_{xy}, (b) d_{xz}, and (c) d_{yz} states, in pristine FeSe (blue lines) and in our model (red lines).

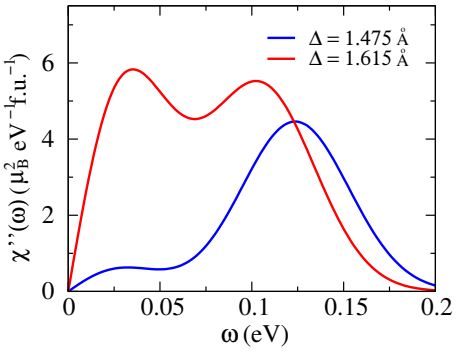

Figure 6. Local spin susceptibility of pristine FeSe (blue line) and of our model (red line).

The increasing of the chalcogen height has considerable effects in the electronic correlations of this material. As shown in Fig. 5, the $\mathrm{Im}\Sigma_\alpha(\omega = 0)$ ($\alpha = \{d_{xy}, d_{xz}, d_{yz}\}$) is enhanced with the increasing Se height. In particular, the d_{xy} states have more profound changes as can be seen in Fig. 5(a). This leads to important broadening effects in the states of d_{xy}, d_{xz}, and d_{yz} character around the Fermi level as can be seen in the single-particle spectral function shown in Fig.2(b) of the main text. These results are consistent with experimental observations, where the single particle spectral function is more coherent in FeSe and becomes more and more incoherent towards to FeTe [20–22]. The enhancement of correlations also leads to important effects on spin ex-

citations. In Fig. 6 we show the imaginary part of the local spin susceptibility obtained from our DMFT calculations. As can be noticed, the low-energy peak located around 0.03 eV is strongly enhanced due to the increasing of Se height. This indicates that the enhancement of correlations is accompanied by a substantial increase of low-energy spin excitations, which again is in agreement with previous inelastic neutron studies [23, 24].

* hmiao@bnl.gov
† dingh@iphy.ac.cn

[1] K. Okazaki, Y. Ito, Y. Ota, Y. Kotani, T. Shimojima, T. Kiss, S. Watanabe, C.-T. Chen, S. Niitaka, T. Hanaguri, H. Takagi, A. Chainani, and S. Shin, **4**, 4109 (2014).
[2] P. Zhang, K. Yaji, T. Hashimoto, Y. Ota, T. Kondo, K. Okazaki, Z. Wang, J. Wen, G. D. Gu, H. Ding, and S. Shin, Science **360**, 182 (2018).
[3] S. Rinott, K. B. Chashka, A. Ribak, E. D. L. Rienks, A. Taleb-Ibrahimi, P. Le Fevre, F. Bertran, M. Randeria, and A. Kanigel, Science Advances **3** (2017), 10.1126/sciadv.1602372.
[4] P. D. Johnson, H.-B. Yang, J. D. Rameau, G. D. Gu, Z.-H. Pan, T. Valla, M. Weinert, and A. V. Fedorov, Phys. Rev. Lett. **114**, 167001 (2015).
[5] M. Chen, X. Chen, H. Yang, Z. Du, X. Zhu, E. Wang, and H.-H. Wen, Nature Communications **9**, 970 (2018).
[6] H. Miao, T. Qian, X. Shi, P. Richard, T. K. Kim, M. Hoesch, L. Y. Xing, X.-C. Wang, C.-Q. Jin, J.-P. Hu, and H. Ding, Nat Commun **6** (2015).
[7] D. L. Feng, D. H. Lu, K. M. Shen, C. Kim, H. Eisaki, A. Damascelli, R. Yoshizaki, J.-i. Shimoyama, K. Kishio, G. D. Gu, S. Oh, A. Andrus, J. O'Donnell, J. N. Eckstein, and Z.-X. Shen, Science **289**, 277 (2000).
[8] H. Ding, J. R. Engelbrecht, Z. Wang, J. C. Campuzano, S.-C. Wang, H.-B. Yang, R. Rogan, T. Takahashi, K. Kadowaki, and D. G. Hinks, Phys. Rev. Lett. **87**, 227001 (2001).
[9] K. Terashima, Y. Sekiba, J. H. Bowen, K. Nakayama, T. Kawahara, T. Sato, P. Richard, Y.-M. Xu, L. J. Li, G. H. Cao, Z.-A. Xu, H. Ding, and T. Takahashi, Proceedings of the National Academy of Sciences **106**, 7330 (2009).
[10] K. Nakayama, T. Sato, P. Richard, Y.-M. Xu, T. Kawahara, K. Umezawa, T. Qian, M. Neupane, G. F. Chen, H. Ding, and T. Takahashi, Phys. Rev. B **83**, 020501 (2011).
[11] H. Ding, P. Richard, K. Nakayama, K. Sugawara, T. Arakane, Y. Sekiba, A. Takayama, S. Souma, T. Sato, T. Takahashi, Z. Wang, X. Dai, Z. Fang, G. F. Chen, J. L. Luo, and N. L. Wang, EPL (Europhysics Letters) **83**, 47001 (2008).
[12] N. Xu, P. Richard, X. Shi, A. van Roekeghem, T. Qian, E. Razzoli, E. Rienks, G.-F. Chen, E. Ieki, K. Nakayama, T. Sato, T. Takahashi, M. Shi, and H. Ding, Phys. Rev. B **88**, 220508 (2013).
[13] N. Xu, P. Richard, X.-P. Wang, X. Shi, A. van Roekeghem, T. Qian, E. Ieki, K. Nakayama, T. Sato, E. Rienks, S. Thirupathaiah, J. Xing, H.-H. Wen, M. Shi, T. Takahashi, and H. Ding, Phys. Rev. B **87**, 094513 (2013).
[14] Y. Zhang, Z. R. Ye, Q. Q. Ge, F. Chen, J. Jiang, M. Xu, B. P. Xie, and D. L. Feng, Nature Physics **8**, 371 (2012).
[15] H. Miao, P. Richard, Y. Tanaka, K. Nakayama, T. Qian, K. Umezawa, T. Sato, Y.-M. Xu, Y. B. Shi, N. Xu, X.-P. Wang, P. Zhang, H.-B. Yang, Z.-J. Xu, J. S. Wen, G.-D. Gu, X. Dai, J.-P. Hu, T. Takahashi, and H. Ding, Phys. Rev. B **85**, 094506 (2012).
[16] Z.-H. Liu, P. Richard, K. Nakayama, G.-F. Chen, S. Dong, J.-B. He, D.-M. Wang, T.-L. Xia, K. Umezawa, T. Kawahara, S. Souma, T. Sato, T. Takahashi, T. Qian, Y. Huang, N. Xu, Y. Shi, H. Ding, and S.-C. Wang, Phys. Rev. B **84**, 064519 (2011).
[17] X.-P. Wang, T. Qian, P. Richard, P. Zhang, J. Dong, H.-D. Wang, C.-H. Dong, M.-H. Fang, and H. Ding, EPL (Europhysics Letters) **93**, 57001 (2011).
[18] D. Liu, C. Li, J. Huang, B. Lei, L. Wang, X. Wu, B. Shen, Q. Gao, Y. Zhang, X. Liu, Y. Hu, Y. Xu, A. Liang, J. Liu, P. Ai, L. Zhao, S. He, L. Yu, G. Liu, Y. Mao, X. Dong, X. Jia, F. Zhang, S. Zhang, F. Yang, Z. Wang, Q. Peng, Y. Shi, J. Hu, T. Xiang, X. Chen, Z. Xu, C. Chen, and X. J. Zhou, **2**, 1 (2018), arXiv:1802.02940v1.
[19] J.-X. Yin, Z. Wu, J.-H. Wang, Z.-Y. Ye, J. Gong, X.-Y. Hou, L. Shan, A. Li, X.-J. Liang, X.-X. Wu, J. Li, C.-S. Ting, Z.-Q. Wang, J.-P. Hu, P.-H. Hor, H. Ding, and S. H. Pan, Nat Phys **11**, 543 (2015).
[20] E. Ieki, K. Nakayama, Y. Miyata, T. Sato, H. Miao, N. Xu, X.-P. Wang, P. Zhang, T. Qian, P. Richard, Z.-J. Xu, J. S. Wen, G. D. Gu, H. Q. Luo, H.-H. Wen, H. Ding, and T. Takahashi, Phys. Rev. B **89**, 140506 (2014).
[21] P. Zhang, T. Qian, P. Richard, X. P. Wang, H. Miao, B. Q. Lv, B. B. Fu, T. Wolf, C. Meingast, X. X. Wu, Z. Q. Wang, J. P. Hu, and H. Ding, Phys. Rev. B **91**, 214503 (2015).
[22] Z. P. Yin, K. Haule, and G. Kotliar, Phys. Rev. B **86**, 195141 (2012).
[23] P. Dai, Rev. Mod. Phys. **87**, 855 (2015).
[24] Q. Wang, Y. Shen, B. Pan, X. Zhang, K. Ikeuchi, K. Iida, A. D. Christianson, H. C. Walker, D. T. Adroja, M. Abdel-Hafiez, X. Chen, D. A. Chareev, A. N. Vasiliev, and J. Zhao, Nature Communications **7**, 12182 (2016).